# RE-SUBMITTED MANUSCRIPT

**JOURNAL OF GLACIOLOGY**

**JAN.-1, 2014**

# Interannual Changes of the Floating Ice Shelf of Petermann Gletscher, North Greenland from 2000 to 2012

Andreas MÜNCHOW,[1] Laurie PADMAN,[2] Helen A. FRICKER,[3]

[1] *College of Earth, Ocean and Environment, University of Delaware, Newark, Delaware, USA*
*E-mail: muenchow@udel.edu*
[2] *Earth & Space Research, Corvallis, OR, USA*
[3] *Scripps Institution of Oceanography, University of California, San Diego, CA, USA*

**ABSTRACT. Petermann Gletscher, NW Greenland, drains 4% of the Greenland Ice Sheet into Nares Strait. Its floating ice shelf retreated from 81 km to 46 km length during two large calving events in 2010 and 2012. We investigate the ice shelf structure during the last decade by using repeat-track airborne topographic mapping and radar, ICESat laser altimetry, and MODIS visible imagery. The steady-state along-flow ice divergence represents 6.3 Gt $a^{-1}$ mass loss through basal melting ($\sim$5 Gt $a^{-1}$) and surface melting and sublimation ($\sim$1.0 Gt $a^{-1}$). Airborne laser altimeter data reveal thinning $\partial H/\partial t$ both along a thin central channel and a thicker ambient ice shelf. From 2007 to 2010 the ice shelf thins by $\sim$5.0 m $a^{-1}$ which represents a non-steady mass loss of about 4.1 Gt $a^{-1}$. We posit that thinning in the already thin basal channels structurally weakened the ice shelf and may have played a role in the recent calving events. The recent ice-shelf velocity, measured by tracking surface features between ATM flights in 2010 and 2011, is $\sim$1.25 km $a^{-1}$, about 15-30% faster than previous estimates.**

## INTRODUCTION

Greenland's tidewater glaciers are losing mass, through thinning and retreat, at an increasing rate (*Joughin et al.*, 2010b; *Howat et al.*, 2011; *Bjork et al.*, 2012). Over the last decade there has been a general clockwise progression of mass loss (*Khan et al.*, 2010; *Chen et al.*, 2011), with initial retreat in south-eastern Greenland (*Luckman et al.*, 2006; *Howat et al.*, 2008) followed by loss in the south-west (*Joughin et al.*, 2004) and, most recently, in north-west Greenland (*Khan et al.*, 2010). In addition to this general trend, there is significant spatial and temporal variability of glacier mass budgets that do not always correlate with readily observed surface forcing (*Howat et al.*, 2011; *Moon et al.*, 2012). These observations support the view that the mass balance of tidewater glaciers is sensitive to the delivery of ocean heat to the submarine portion of the glacier (*Straneo and Heimbach*, 2013).

Many tidewater glaciers in Greenland north of 78° N terminate in ice shelves, floating extensions of the glaciers extending up to several tens of km into the adjacent fjords (*Rignot et al.*, 2001). Based on recent observations in Antarctica and Greenland, we expect that reduction in size and thinning of these ice shelves could cause accelerated dynamic loss of adjacent grounded ice and consequent sea level rise (*Scambos et al.*, 2004; *Holland et al.*, 2008; *Nick et al.*, 2013). While most North Greenland ice shelves have been relatively stable, Academy and C.H Ostenfeld Gletscher lost their floating ice shelves in the 1950ies (*Higgins*, 1991) and in 2001 (*Joughin et al.*, 2010a), respectively. Zachariæ Isstrøm retreated from its slow-moving, landfast ice shelf in 2012/13 after two decades of retreat while Petermann Gletscher lost well over a quarter of its ice shelf in 2010 and 2012 (*Johnson et al.*, 2011; *Nick et al.*, 2013). What remains of Greenland's ice shelves is threatened by a changing climate, because both regional air (*Chylek et al.*, 2009) and ocean temperatures (*Zweng and Münchow*, 2006; *Polyakov et al.*, 2010; *Münchow et al.*, 2011) continue to increase while Arctic sea ice cover continues to decline (*Stroeve et al.*, 2012).

In 2010 Petermann Gletscher (hereafter denoted PG) in North Greenland discharged a Manhattan-sized ice island (Figure 1). Within days the United States Congress held formal hearings on this event to investigate its climate change implications. Subsequently, *Johnson et al.* (2011) reported on ocean waters and circulation in Petermann Fjord while *Nick et al.* (2012) introduced 2006-12 glacier velocities and modeled how the glacier may respond to the 2010 calving event. Both studies cautioned against public perceptions that this is caused by globally warming air temperatures. Nevertheless, an equally large 2012 calving motivated us to here provide a detailed description on how this ice shelf varied in all three spatial dimensions and how it evolved in time during the last decade. We thus provide context for more integrated future ice, ocean, glacier interaction studies.

PG drains about 69,000 $km^2$ (*Rignot et al.*, 2001) of the 1,710,000 $km^2$ Greenland Ice Sheet, i.e., about $\sim$4%. Historically it terminates in a 70 long, 15 km wide, and 300 m thick floating ice shelf. The glacier is grounded at $\sim$600 m depth below current sea level (*Rignot and Steffen*, 2008). It deepens for another 20 km upstream and its bed rock is below current sea level for another 60 km inland (*Bamber et al.*, 2013; *Rignot*, 1998).

PG moves steadily seaward at a reported average rate of between 0.95 km $a^{-1}$ (*Higgins*, 1991) and 1.1 km $a^{-1}$ (*Rignot*

*and Steffen*, 2008), with a weak seasonal modulation of about 0.1 km $a^{-1}$ (*Nick et al.*, 2012). The total annual discharge at the grounding line is 12±1 Gt $a^{-1}$(*Rignot and Steffen*, 2008). *Higgins* (1991) estimated the long-term mean calving rate at ∼0.6 Gt $a^{-1}$ or about 5% of the flux across the grounding line. Annual precipitation is small, and the ice shelf surface undergoes net mass loss of 1.2 m $a^{-1}$ (1.3 Gt $a^{-1}$ for a mean ice shelf area of 1300 $km^2$) through winter sublimation and summer melting (*Rignot and Steffen*, 2008; *Rignot et al.*, 2001). If the glacier is in a steady state, then about ∼85% of the mass loss occurs via basal melting. Sufficient ocean heat is available inside the fjord to reach the sub-ice-shelf cavity (*Johnson et al.*, 2011; *Rignot et al.*, 2012). This heat originates from adjacent Nares Strait whose Atlantic layer waters have been warming for the last decade (*Münchow et al.*, 2011). *Gladish et al.* (2012) developed a model of ice-ocean interactions that generated basal melt rates that ranged from 25 m $a^{-1}$ at the grounding line to zero at the ice front. These model results were generally consistent with the observations of *Rignot and Steffen* (2008).

Two large calving events at PG in 2010 and 2012 reduced the length of the ice shelf length from 81 km to 46 km (Figures 1 and 2). While PG has experienced large calving events in the past (*Falkner et al.*, 2011), its terminus (ice front) has now retreated farther back than has previously been observed since the first reported measurements were made in 1876 (*Nares*, 1876). By analogy with Jakobshavn Isbrae (*Motyka et al.*, 2011), it is possible that loss of the PG ice shelf would lead to significant and rapid mass loss of grounded ice. We note, however, that the dramatic collapse of the ice shelf of Jakobshavn Isbrae took place more than 1000 km to the south where ocean waters of Atlantic origin (*Zweng and Münchow*, 2006) caused enhanced basal melting (*Holland et al.*, 2008). Furthermore, *Nick et al.* (2012, 2013) argue that PG will not accelerate even with large fractions of its ice shelf removed. Future observations will bear out this prediction. We here describe how Petermann's floating ice shelf has evolved over the last decade in all three spatial dimensions.

## DATA AND METHODS

NASA conducted overflights of PG using DC-8 (2010) and P-3 (2002, 2003, 2007, and 2011) aircraft. The planes carried a multi-channel radar depth sounder operated by the University of Kansas to estimate the location of the air-ice and ice-ocean or ice-bedrock interfaces to determine ice thickness at about 100-m horizontal resolution (*Gogineni et al.*, 2001). The planes also carried an airborne topographic mapper (ATM) which is a scanning light detection and ranging laser (*Krabill et al.*, 2002). We use level 1B ATM data (*Krabill*, 2010) with spatial resolution of ∼1 m, but apply a Lanczos low-pass filter to longitude, latitude, and elevation to generate an along-track series to represent features at scales above ∼300 m at ∼30 m spacing. Two lines were repeated in multiple years that were separated across-fjord by ∼1.5 km (Figure 1). The western line followed a 100-m narrow surface channel. The eastern line is over thicker ice that is more typical of the ice shelf.

We also obtained elevation data from the Geoscience Laser Altimeter System (*Shuman et al.*, 2006) on NASA's Ice, Cloud and land Elevation Satellite (ICESat) for four tracks that cross the fjord (Figure 1). Up to ten cloud-free repeat orbits were acquired for each track from 2003 through 2008. ICESat acquired elevation estimates every ∼170 m along its track, with a footprint diameter of ∼50-100 m. Data processing follows protocols described by *Padman et al.* (2008) and *Fricker et al.* (2009).

We converted GPS location for ATM, radar, and ICESat data from a WGS-84 ellipsoid to EGM2008 geoid reference (*Pavlis et al.*, 2012); this correction is 12-20 m in our study area. We corrected for tidal elevation using predictions from the AOTIM5 tide model (*Padman and Erofeeva*, 2004). This model does not resolve Petermann Fjord, therefore we used a model grid point at the entrance to the fjord rather than locations of actual elevation measurements. We speculate that additional tidal variability inside the fjord is negligible, because the barotropic tidal wave propagates in and out of the fjord within 10 minutes. Frictional forces under the floating ice shelf will change both tidal amplitude and propagation, but these are difficult to assess without a dynamical model or without knowledge of ocean current, bottom depth, or ice shelf topography. *Reeh et al.* (2000) finds tidal amplitudes under the 60 km long ice shelf of Nioghalvfjerdsfjorden off northeastern Greenland to vary less than 20% near the grounding line as compared to the forcing open ocean tide which at Petermann would correspond to a tidal uncertainty of less than 0.1 m.

For radar, we removed an unknown radar offset bias by assuming a hydrostatic balance of a 30 km floating section of the ice shelf. Using an approach similar to (*Bindschadler et al.*, 2011), we fit estimates of ice thickness $H$ from the radar to

$$Z = offset + ratio \times H \tag{1}$$

where $Z$ is the surface elevation from the radar above the geoid. The regression coefficients "offset" and "ratio" are determined via least-squares and represent, respectively, an unknown radar offset and a buoyancy ratio. If the ice shelf is floating and in hydrostatic balance, then $ratio = (1 - \rho_{ice}/\rho_{water}) = 0.106$ for an ice density $\rho_{ice}$=917 kg $m^{-3}$ and an ocean density $\rho_{ice}$=1026 kg $m^{-3}$. The offset includes an unknown firn-air correction (*Bindschadler et al.*, 2011); however, this correction should be negligible for PG because annual snowfall is small compared with surface mass loss through melting and sublimation (see next section). Table 1 lists these regression coefficients along with pertinent details of aircraft surveys conducted over PG since 2002. The buoyancy ratio is close to the expected value for the ambient ice shelf, but deviates somewhat for the central channel.

The radar-based estimates of the depth of the ice base (draft) are accurate to within 10 m (*Gogineni et al.*, 2001), and the concurrent ATM estimates of the location of the ice surface (elevation) are accurate to ∼0.2 m (*Krabill et al.*, 2002). Assuming hydrostatic balance, we convert these elevations to draft to determine (a) the location of the grounding line and (b) deviations from hydrostatic balance (*Bindschadler et al.*, 2011).

No radar data are available concurrent with ICESat elevation measurements, therefore we cannot test the hydrostatic assumption for these data.

# RESULTS

## Changes in ice shelf extent

The surface evolution of the glacier and the ice islands it spawned are indicated by MODIS imagery from the summers of 2003, 2010, and 2012 (Figure 1). During the 2003-2010 period the glacier's terminus advanced about 6 km (to y≈80 km; see Figure 1) even though, in 2008, two smaller calving events removed 30 km$^2$ of ice shelf (not shown).

The calving front reached y=80 km seaward of the grounding line (Figures 1 and 3) before shedding 253±17 km$^2$ on August 4, 2010. A further 130±10 km$^2$ was calved on July 16, 2012. Areal estimates are based on manually counting MODIS pixels on paper while the uncertainty is due to partial pixels and semi-detached areas of the ice island. Figure 3 show surface elevation from ATM and bottom topography from radar for a repeat airborne survey in the springs of 2010 (March 24) and 2011 (May 7) $\delta t$=408 days apart. The profile from 2010 has been shifted seaward by $\delta x$=1.4 km relative to the 2007 profile and results in the largest (spatially lagged) correlation between the two profiles; this shift corresponds to an average speed of V=$\delta x/\delta t$ = 1.25 km a$^{-1}$. The shift reveals high spatial correlation of surface elevation and bottom draft as features are advected downstream. The inferred glacier speed is ∼30% higher than previously published estimates by *Higgins* (1991) and *Rignot and Steffen* (2008), but falls within the values given by *Nick et al.* (2012) during the 2006-11 period.

The segment of the ice shelf that broke off in 2010 was 69±6.0 m thin while the 2012 ice island was 161±2.6 m thick (Figure 3 where the uncertainty is a standard deviation. Using these along-shelf profiles and assuming a realistic ice thickness profile across the glacier (to be discussed below), we find that similar mass was lost during each of the two calving events in 2010 and 2012, about 18±2 Gt for each event.

After the 2012 calving the ice shelf reached its shortest extent in the historical record, which begins in 1876; see Figure 1b in *Falkner et al.* (2011) and updated to end of 2012 in our Figure 2.

## Elevation variability

Elevations of PG vary substantially both along and across the ice shelf on scales of order 1 km and less: Figure 4) shows this variability with ICESat data across glacier while Figure 3 demonstrates variations with ATM data along the glacier. Some features are apparent:

First, across-glacier tracks of ICESat elevation from 2003 through 2008 cross a deep channel near the middle of the ice shelf. This channel coincides with the western trackline flown by aircraft surveys and it is most pronounced at ICESat track 220, ∼15 km seaward of the grounding line (Figure 4). While the location of this this channel does not vary laterally (see discussion below), its elevation decreases from a maximum of 18 m in November 2003 to a minima of 6 and 8 m in March of 2004 and 2007, respectively (Figures 4 and 5). Linear trends from point measurements of elevation change over time are generally not significantly different from zero; however, the along-track (across-shelf) average over the central section of the ice shelf thinned at a rate of 0.33 ±0.26 m a$^{-1}$ (Figure 5); the uncertainty represents a 95% confidence limit in linear regression (*Fofonoff and Bryden*, 1975). This section includes both the central channel and the ambient ice shelf to its east and west.

Second, the elevation of the ambient ice shelf on either side of the central channel varies greatly: the western ambient ice shelf is 10-25 % thicker than the ice shelf to the east. For track 220 the time-mean, spatially averaged thickness is 33±6.0 m and 31±11.7 m to the west and east of the central channel, respectively (Table 3). The ice draft along the central channel is always less than half the ambient ice shelf thickness; cf. *Rignot and Steffen* (2008).

Third, we can trace the central channel seaward towards the terminus in ICESat tracks 101 and 1336 as it becomes broader and exhibits less variability in elevation (Table 3). The channel is also visible towards the grounding line in both ICESat track 399 as well as in optical imagery that we discuss next to demonstrate the channel's stationarity in both time and space.

Gradients of surface elevations cause variations in surface reflectance in remotely sensed optical MODIS imagery (Figure 1). For similar sun and satellite angles the spatial gradients of reflectance fall at similar locations (*Bindschadler et al.*, 2010; *Scambos et al.*, 2007). We construct a time series of reflectance gradients from one cloud-free MODIS Terra image taken within 135 minutes of 20:50 UTC between April 30 and May 20 for each year from 2000 to 2012. Figure 6 shows the absolute magnitude of the reflectance gradient vector for an across-shelf section located 15 km seaward from the grounding line near ICESat track 220. The central channel appears as a stationary feature that does not move laterally by more than one pixel (250 m) throughout the 12-year record. It also reveals a distinct secondary peak gradient to the east of the central channel (x∼83 km) that is also visible at this general location in ICESat elevation data (Figure 4) about 4-5 km to the east of the central channel.

Profiles from repeat airborne surveys along the fjord with two flight lines spaced 1.5 km apart allow us to further investigate elevation and ice thickness change (Table 1). The elevation along these tracks in 2002 (Figure 7) shows that the central (west) channel extends from the grounding line at least 50 km seaward, remaining roughly half the thickness of the ambient ice shelf (east transect) for much of this range.

## Hydrostatics

Assuming hydrostatic balance, we estimate along-shelf draft from the ATM-derived elevations shown in Figure 7. Correcting for the geoid and tides, we compare this hydrostatic ice bottom with that measured by ice penetrating radar. For the ambient ice shelf, the agreement between this estimate and that obtained from coincident radar data is excellent (Figure 7, middle panel) as a correlation coefficient $r^2$=0.993 gives us confidence in both ice surface (ATM) and bottom (radar) measurements as well as the validity of the hydrostatic assumption. Deviations from this balance near the grounding line indicate the location where the glacier sits on bedrock rather than being afloat (*Bindschadler et al.*, 2011). Figure

7 suggests a grounding zone near 2 km in our coordinate system, consistent with *Rignot and Steffen* (2008) based on 2002 and 2003 radar data.

The same analysis applied to the 2002 transect along the central channel (Figure 7, bottom panel) shows similar agreement along most of the flight line; the exception is a ∼5 km long region where the radar-derived ice draft is much deeper than the hydrostatic value. ICESat track 220 crosses this region (Figure 4), showing that the minimum elevation in the central channel declined from ∼18 m to ∼8 m by 2007 (Figure 5b). The reported ice thickness from the radar is comparable to ice thickness of the ambient ice shelf at the same distance along the fjord; therefore, we tentatively interpret this region as an extremely narrow basal channel that cannot be resolved by the airborne radar, so that the radar returns come from the ice base on either side of the channel. Given that the ice thickness in the channel (∼150 m) is comparable to the width of the channel, it is also likely that the force balance for the ice across the channel is not simply hydrostatic but includes some bridging stresses.

Comparison of data from the two flight lines (Figure 7) indicates substantial variation in both thickness and surface elevation across the glacier, consistent with the ICESat cross-glacier elevation transects (Figure 4). Ambient ice-shelf thickness ranges from about 550 m at the grounding line to 80 m at its front (Figure 7, middle panel), but lateral ice thickness gradients often exceed 100 m over the 1.5 km separation of the two tracks. During summer, meltwater ponds frequently form everywhere on the floating ice shelf, and a meandering central channel is often filled with water at the surface that is easily visible in high resolution optical imagery. If crevasses or other pathways for downward propagation of surface-produced freshwater exist along the central channel, this freshwater may be provided directly to the sub-ice-shelf cavity or provide impetus for hydrofracture (*Scambos et al.*, 2000; *Vaughan et al.*, 2012).

## Ice thickness change with time

Analyses of elevation from repeated measurements along ICESat track 220 (Figures 4 and 5) suggest that the ice shelf is thinning at that location by about ∼3.1±2.4 m $a^{-1}$. Assuming this value applied to the entire ice shelf, it would account for 4.8 Gt $a^{-1}$ or about 40% of the total loss of mass from the 12 Gt $a^{-1}$ crossing the grounding line.

The repeated track lines flown by NASA aircraft in 2002, 2007, and 2010 allow us to check the assumption that this thinning is extensive. These repeat lines were always within 300 m of each other with a root-mean-square deviation of 63 m and 73 m for the track over the central channel and the ambient ice shelf, respectively (not shown). From the transects of MODIS surface reflectance gradients (Figure 6), there was negligible cross-stream migration of the central channel during this period. The radar ice draft data for these three years (Figure 8b) show dramatic changes in the central channel within ∼10 km of the grounding line. Radar-estimated ice draft changed from 400 m in 2002 and 2007 to ∼100-150 m in 2010. The ambient ice shelf showed no change except for the downstream migration of $O(100)$ m high perturbations in the ice base (Figure 8a).

We will next use these radar and corresponding ATM elevation data to quantify ice thickness change along these aircraft transects. Using only surface elevation data from the ATM, we define an average hydrostatic ice thickness $\widehat{H}$ as the integral from near the grounding line at $y_1 = 2$ km to some distance $y_2 > y_1$ km along the ice shelf with $L = y_2 - y_1$, e.g.,

$$\widehat{H}(x,t) = 1/L \int_{y_1}^{y_2} H(x,y,t)\, dy \tag{2}$$

This reduces the noise of point-by-point elevation comparisons of a moving ice shelf with rough surface topography such as PG (*Thomas et al.*, 2009; *Schenk and Csatho*, 2012).

Figure 9 shows $W \times \widehat{H}$ and $H(y)$ for the central channel and the ambient ice shelf for 2007 and 2010 where $W$ is the width of the fjord (∼18-20 km). Taking the 2012 terminus location as the limit, i.e., $y_2 = 48$ km, we find that the value of $\widehat{H}$ decreases from 216 m in 2007 to 203 m in 2010 for the central channel, and from 352 m to 339 m on the ambient ice shelf for the same period (Figure 9, top panel; Table 4). The floating ice shelf thus thinned by 13 m, averaged along ice flowlines from 2007 to 2010. Note that the 2007 observations were taken in the summer after some seasonal surface melting has taken place while the 2010 observations were taken in the spring when no surface melting takes place.

Based on this comparison, the annual rate of hydrostatic thinning from 2007 to 2010 is 5.0 m $a^{-1}$ for both the ambient ice shelf and the central channel. This corresponds to a reduced surface elevation of about 0.53 m $a^{-1}$ and compares to both the linear trend of ICESat across-shelf averaged elevation data of -0.33 ±0.26 m $a^{-1}$ (Figure 5, Table 4) and the regional value of -0.25±0.06 m $a^{-1}$ estimated by *Gardner et al.* (2013) for all of North Central Greenland.

## DISCUSSION

The vertically averaged conservation of mass gives

$$\partial H/\partial t + \nabla(\vec{u}H) = \dot{a} - \dot{m} \tag{3}$$

where H is the thickness of the ice, $\vec{u} = (u, v)$ is vertically averaged velocity vector with across- and along-stream components u and v, $\dot{a}$ is the difference between surface ablation and accumulation, and $\dot{m}$ is the basal melt.

We first consider the steady state mass balance, i.e., $\partial H/\partial t = 0$. Since the nonlinear dynamic thinning $H\nabla\vec{u}$ is small (*Higgins*, 1991) and the across-stream flow is negligible, equation (3) simplifies to

$$v_0\, \partial H/\partial y = \dot{a} - \dot{m} \tag{4}$$

Using this result, we estimate a net melt rate, $\dot{a} - \dot{m}$, from thickness variations $H$ along the ice shelf and a constant along-shelf velocity that we take as 1.25 km $a^{-1}$ that we found by feature tracking along repeat flight lines from 2010 to 2011 (Figure 3). We subsample the irregularly spaced ice thickness profile into a constant along-glacier grid with $\delta y = 50$ m resolution. This minimizes numerical artifacts when estimating the gradient $\partial H/\partial y$ and net melt-rate from Equation (4).

Net steady-state melt rate $v_0\,\partial H/\partial y$ varies from about 18 m a$^{-1}$ near the grounding line to the surface ablation rate $\dot{a} \simeq$ 1.2 m a$^{-1}$ at the terminus (Figure 9). Averaging these values along each track for $y \in [2, 75]$ km in each year, we find almost identical net melt rates in 2007 and 2010, $\sim$4.9 m a$^{-1}$ for the central channel and $\sim$8.0 m a$^{-1}$ for the ambient shelf (Table 4). The central channel area is about 2 km wide while the ambient shelf covers the remaining 14 km. Hence we partition the ice shelf into 1/8 central channel and 7/8 ambient shelf. Applying these weights to the melt rates, we attribute 6.3 G a$^{-1}$ of ice loss to the steady-state term represented by divergence of the ice volume flux. This is only about half of the 12 Gt a$^{-1}$ ice flux into the fjord at the grounding line *Rignot and Steffen* (2008). The other half is provided by calving and non-steady thinning.

From September 2007 to May 2010, the glacier thinned at a rate $\partial\widehat{H}/\partial t$ of 5.0 m a$^{-1}$ for both the central melt-channel and the ambient shelf (Table 4). These values are of the same order of magnitude as the melt-rates from the steady divergence (Equation 4). We thus conclude that Petermann's ice shelf was not in steady state prior to its extreme 2010 and 2012 calving events. The net melt rate is the sum of the non-steady and steady thinning, e.g.,

$$\partial\widehat{H}/\partial t + v_0 \sum_{k=1}^{N} \partial H(y_k)/\partial y = \dot{a} - \dot{m} \qquad (5)$$

where $\partial H(y_k)/\partial y$ describes the thinning due to the ice divergence estimated along flow lines from 2007 and 2010 data. The net melt rate thus becomes 9.9 m a$^{-1}$ for the central channel and 13.0 m a$^{-1}$ for the ambient floating ice shelf. These numbers agree with those of *Rignot and Steffen* (2008) and *Rignot et al.* (2001); however, we have shown that a significant fraction of this melting is from the non-steady component $\partial H/\partial t$.

The melt rate maxima near the grounding line reach about 20 m a$^{-1}$ in our calculations. These are about 20% smaller than those observed in 2002/2003 by *Rignot and Steffen* (2008), who used the full velocity divergence $\nabla(\vec{u}H)$ and the ice thickness field was measured by the ice profiling radar along 10 along-glacier flight lines. In contrast, we here used hydrostatic ice thickness derived from surface elevation ATM data along just 2 repeat lines. We hypothesize that the discrepancy arises because (a) the mass balance of the ice shelf is not always in steady state at interannual time scales and (b) not all segments of the ice shelf are in hydrostatic balance, so that errors arise through interpreting surface elevation changes as hydrostatically-compensated thickness changes.

We noted above that some sections of the along-flowline transects of ice draft show large basal crevasses (Figures 3 and 10). These crevasses can be sufficiently small that they are not hydrostatically balanced. A section along the western wall of Petermann surveyed in 2011 revealed a sequence of 8-10 subsurface crevasses: ice thickness changes from 400 m to 150 m within less than 500 m in the along-flow direction (Figure 10). These undulations occur near the grounding line and do not have surface expressions. They appear similar in form to basal crevasses observed recently at Pine Island Glacier, Antarctica (*Bindschadler et al.*, 2011; *Vaughan et al.*, 2012), but have not previously been observed in North Greenland. Following *Vaughan et al.* (2012), we hypothesize that stresses across these crevasses may contribute to structural weakening of the ice-shelf. They may also impact basal melting; however, we do not know whether the net effect will be to increase or decrease mass loss by basal melting.

## CONCLUSIONS

Analyzing available repeat-track airborne and ICESat laser altimeter data for the 2002-2011 period, we find spatially averaged melt rates of 10-13 m a$^{-1}$ that are consistent with those reported by *Rignot and Steffen* (2008) and modeled by *Gladish et al.* (2012). In contrast to prior studies, however, we find that almost half of this basal melt rate is due to a non-steady response. More specifically, we find the non-steady thinning to vary between 3-5 m a$^{-1}$ during the 2003-2010 period. The larger rates of 5 m a$^{-1}$ are based on evolution of ice thickness 2007 to 2010, while the lower estimate is based on 2003-2009 trends in elevation recorded by ICESat repeat tracks about 15 km north of the grounding line. Trends of ICESat tracks closer to the terminus are not significantly different from zero (not shown); however, the interannual variability on these estimates is larger and the sampling size is smaller, hence we cannot rule out linear trend values similar to track 220.

The role of ice-shelf basal channels and crevasses in net basal melting and ice-shelf structural integrity requires further exploration and modeling (*Sergienko*, 2013). Our analyses suggest similar thinning in the central channel and the ambient ice shelf. We did not find any evidence of cross-fjord migration of this or other channel over the decade for which we have MODIS imagery (Figure 6), suggesting that basal melting within the channel does not occur preferentially to one side of the channel. Further interpretation is hampered by uncertainty in ice thickness measurements from airborne radar under such narrow features, implying the need for repeated surface radar measurements and/or submarine profiling of ice-shelf basal topography (*Vaughan et al.*, 2012).

We conclude that the ice shelf of Petermann Gletscher is not in steady state. Changing ocean temperatures in adjacent Nares Strait (*Münchow et al.*, 2011), ice shelf thickness changes from 2002 to 2011 reported here, and two major calving events in 2010 (*Johnson et al.*, 2011) and 2012 all indicate a potential transition to a new, unknown state.

## ACKNOWLEDGMENTS

We acknowledge financial support from National Science Foundation grant 1022843 (AM) and NASA grant NNX10AG19G (LP), and (HAF). The data and/or data products from CReSIS were generated with support from NSF grant ANT-0424589 and NASA grant NNX10AT68G. Humfrey Melling kindly provided data used in Figure 2. This is ESR contribution XXX.

## REFERENCES

Bamber, J. L., M. J. Siegert, J. A. Griggs, S. J. Marshall, and G. Spada, Paleofluvial mega-canyon beneath the central Greenland ice sheet, *Science*, *341*, 997–999, 2013.

Bindschadler, R., D. G. Vaughan, and P. Vornberger, Variability of basal melt beneath the Pine Island Glacier ice shelf, West Antarctica, *Journal of Glaciology*, *57*, 581–595, 2011.

Bindschadler, R. A., T. A. Scambos, H. Choi, and T. M. Haran, Ice sheet change detection by satellite image differencing, *Remote Sensing of Environment*, *114*, 1353–1362, 2010.

Bjork, A. A., K. H. Kjaer, N. J. Korsgaard, S. A. Khan, K. K. Kjeldsen, C. S. Andresen, J. E. Box, N. K. Larsen, and S. Funder, An aerial view of 80 years of climate-related glacier fluctuations in southeast Greenland, *Nature Geoscience*, *5*, 427–432, 2012.

Chen, J. L., C. R. Wilson, and B. D. Tapley, Interannual variability of Greenland ice losses from satellite gravimetry, *J. Geophys. Res.*, *116*, B07,406, 2011.

Chylek, P., C. K. Folland, G. Lesins, M. K. Dubey, and M. Y. Wang, Arctic air temperature change amplification and the Atlantic Multidecadal Oscillation, *Geophys. Res. Let.*, *36*, L14,801, 2009.

Falkner, K., et al., Context for the recent massive Petermann Glacier calving event, *EOS*, *92*, 117–124, 2011.

Fofonoff, N., and H. Bryden, Density of sea waters, *J. Mar. Res.*, *41*, 69–82, 1975.

Fricker, H. A., R. Coleman, L. Padman, T. A. Scambos, J. Bohlander, and K. M. Brunt, Mapping the grounding zone of the Amery Ice Shelf, East Antarctica using InSAR, MODIS and ICESat, *Antarctic Science*, *21*, 515–532, 2009.

Gardner, A. S., et al., A reconciled estimate of glacier contributions to sea level rise: 2003 to 2009, *Science*, *340*, 852–857, 2013.

Gladish, C. V., D. M. Holland, P. R. Holland, and S. F. Price, Ice-shelf basal channels in a coupled ice/ocean model, *Journal of Glaciology*, *58*, 1227–1244, 2012.

Gogineni, S., et al., Coherent radar ice thickness measurements over the Greenland ice sheet, *J. Geophys. Res.*, *106*, 33,761–33,772, 2001.

Higgins, A., North Greenland glacier velocities and calf ice production, *Polarforschung*, *60*, 1–23, 1991.

Holland, D. M., R. H. Thomas, B. De Young, M. H. Ribergaard, and B. Lyberth, Acceleration of Jakobshavn Isbrae triggered by warm subsurface ocean waters, *Nature Geoscience*, *1*, 659–664, 2008.

Howat, I. M., I. Joughin, M. Fahnestock, B. E. Smith, and T. A. Scambos, Synchronous retreat and acceleration of southeast Greenland outlet glaciers 2000-06: ice dynamics and coupling to climate, *Journal of Glaciology*, *54*, 646–660, 2008.

Howat, I. M., Y. Ahn, I. Joughin, M. R. van den Broeke, J. T. M. Lenaerts, and B. Smith, Mass balance of Greenland's three largest outlet glaciers, 2000-2010, *Geophys. Res. Let.*, *38*, L12,501, 2011.

Johnson, H., A. Münchow, K. Falkner, and H. Melling, Ocean circulation and properties in Petermann Fjord, Greenland, *J. Geophys. Res.*, *116*, C01,003, 2011.

Joughin, I., W. Abdalati, and M. Fahnestock, Large fluctuations in speed on Greenland's Jakobshavn Isbrae glacier, *Nature*, *432*, 608–610, 2004.

Joughin, I., B. E. Smith, and D. M. Holland, Sensitivity of 21st century sea level to ocean-induced thinning of Pine Island Glacier, Antarctica, *J. Geophys. Res.*, *37*, L20,502, 2010a.

Joughin, I., B. E. Smith, I. M. Howat, T. Scambos, and T. Moon, Greenland flow variability from ice-sheet-wide velocity mapping, *Journal of Glaciology*, *56*, 415–430, 2010b.

Khan, S. A., J. Wahr, M. Bevis, I. Velicogna, and E. Kendrick, Spread of ice mass loss into northwest Greenland observed by GRACE and GPS, *Geophysical Research Letters*, *37*, L06,501, 2010.

Krabill, W., IceBridge ATM L1B Qfit elevation and return strength. version 1., *Tech. rep.*, NASA DAAC at the National Snow and Ice Data Center, Boulder, Colorado USA., 2010.

Krabill, W. B., W. Abdalati, E. B. Frederick, S. S. Manizade, C. F. Martin, J. G. Sonntag, R. N. Swift, R. H. Thomas, and J. G. Yungel, Aircraft laser altimetry measurement of elevation changes of the Greenland Ice Sheet: technique and accuracy assessment, *Journal of Geodynamics*, *34*, 357–376, 2002.

Luckman, A., T. Murray, R. de Lange, and E. Hanna, Rapid and synchronous ice-dynamic changes in East Greenland, *Geophys. Res. Let.*, *33*, L03,503, 2006.

Moon, T., I. Joughin, B. Smith, and I. Howat, 21st-century evolution of Greenland outlet glacier velocities, *Science*, *336*, 576–578, 2012.

Motyka, R. J., M. Truffer, M. Fahnestock, J. Mortensen, S. Rysgaard, and I. Howat, Submarine melting of the 1985 Jakobshavn Isbrae floating tongue and the triggering of the current retreat, *J. Geophys. Res.*, *116*, F01,007, 2011.

Münchow, A., K. K. Falkner, H. Melling, B. Rabe, and H. L. Johnson, Ocean warming of Nares Strait bottom waters off northwest Greenland, 2003-2009, *Oceanography*, *24*, 114–123, 2011.

Nares, G., *The official report of the recent Arctic expedition*, J. Murray, London, 1876.

Nick, F. M., A. Luckman, A. Vieli, C. J. Van Der Veen, D. Van As, R. S. W. Van De Wal, F. Pattyn, A. L. Hubbard, and D. Floricioiu, The response of Petermann Glacier, Greenland, to large calving events, and its future stability in the context of atmospheric and oceanic warming, *Journal of Glaciology*, *58*, 229–239, 2012.

Nick, F. M., A. Vieli, M. L. Andersen, I. Joughin, A. Payne, T. L. Edwards, F. Pattyn, and R. S. W. van de Wal, Future sea-level rise from Greenland's main outlet glaciers in a warming climate, *Nature*, *497*, 235–238, 2013.

Padman, L., and S. Erofeeva, A barotropic inverse tidal model for the Arctic Ocean, *Geophys. Res. Let.*, *31*, L02,303, 2004.

Padman, L., S. Y. Erofeeva, and H. A. Fricker, Improving Antarctic tide models by assimilation of ICESat laser altimetry over ice shelves, *Geophys. Res. Let.*, *35*, L22,504, 2008.

Pavlis, N. K., S. A. Holmes, S. C. Kenyon, and J. K. Factor, The development and evaluation of the Earth Gravitational Model 2008 (EGM2008), *J. Geophys. Res.*, *117*, B04,406, 2012.

Polyakov, I. V., et al., Arctic ocean warming contributes to reduced polar ice cap, *J. Phys. Oceanogr.*, *40*, 2743–2756, 2010.

Reeh, N., C. Mayer, O. B. Olesen, E. L. Christensen, and H. H. Thomsen, Tidal movement of Nioghalvfjerdsfjorden Glacier, northeast Greenland: observations and modelling, *Annals of Glaciology, Vol 31, 2000*, *31*, 111–117, 2000.

Rignot, E., Hinge-line migration of Petermann Gletscher, north Greenland, detected using satellite-radar interferometry, *Journal of Glaciology*, *44*, 469–476, 1998.

Rignot, E., and K. Steffen, Channelized bottom melting and stability of floating ice shelves, *Geophys. Res. Let.*, *35*, L02,503, 2008.

Rignot, E., S. Gogineni, I. Joughin, and W. Krabill, Contribution to the glaciology of northern Greenland from satellite radar interferometry, *J. Geophys. Res.*, *106*, 34,007–34,019, 2001.

Rignot, E., I. Fenty, D. Menemenlis, and Y. Xu, Spreading of warm ocean waters around Greenland as a possible cause for glacier acceleration, *Ann. Glaciol.*, *53(60)*, 257–266, 2012.

Scambos, T., J. Bohlander, C. Shuman, and P. Skvarca, Glacier acceleration and thinning after ice shelf collapse in the Larsen B embayment, Antarctica, *Geophys. Res. Let.*, *31*, 2004.

Scambos, T. A., C. Hulbe, M. Fahnestock, and J. Bohlander, The link between climate warming and break-up of ice shelves in the Antarctic Peninsula, *Journal of Glaciology*, *46*, 516–530, 2000.

Scambos, T. A., M. Fahnestock, T. Haran, and J. Bohlander, A MODIS-based mosaic of Antarctica, *Remote Sens. Environ.*, *11*, 242–257, 2007.

Schenk, T., and B. Csatho, A new methodology for detecting ice sheet surface elevation changes from laser altimetry data, *IEEE Trans. Geosci. Remote Sens.*, *50*, 3302–3316, 2012.

Sergienko, O. V., Basal channels on ice shelves, *J. Geophys. Res.*, *118*, 1342–1355, 2013.

Shuman, C. A., H. J. Zwally, B. E. Schutz, A. C. Brenner, J. P. DiMarzio, V. P. Suchdeo, and H. A. Fricker, ICESat Antarctic elevation data: Preliminary precision and accuracy assessment, *Geophys. Res. Let.*, *33*, L07,501, 2006.

Straneo, F., and P. Heimbach, North Atlantic warming and the retreat of Greenland's outlet glaciers, *Nature*, *504*, 36–43, 2013.

Stroeve, J. C., M. C. Serreze, M. M. Holland, J. E. Kay, J. Malanik, and A. P. Barrett, The arctic's rapidly shrinking sea ice cover: a research synthesis, *Climatic Change*, *110*, 1005–1027, 2012.

Thomas, R., E. Frederick, W. Krabill, S. Manizade, and C. Martin, Recent changes on Greenland outlet glaciers, *Journal of Glaciology*, *55*, 147–162, 2009.

Vaughan, D. G., H. F. J. Corr, R. A. Bindschadler, P. Dutrieux, G. H. Gudmundsson, A. Jenkins, T. Newman, P. Vornberger, and D. J. Wingham, Subglacial melt channels and fracture in the floating part of Pine Island Glacier, Antarctica, *J. Geophys. Res.*, *117*, F03,012, 2012.

Zweng, M. M., and A. Münchow, Warming and freshening of Baffin Bay, 1916-2003, *J. Geophys. Res.*, *111*, C07,016, 2006.

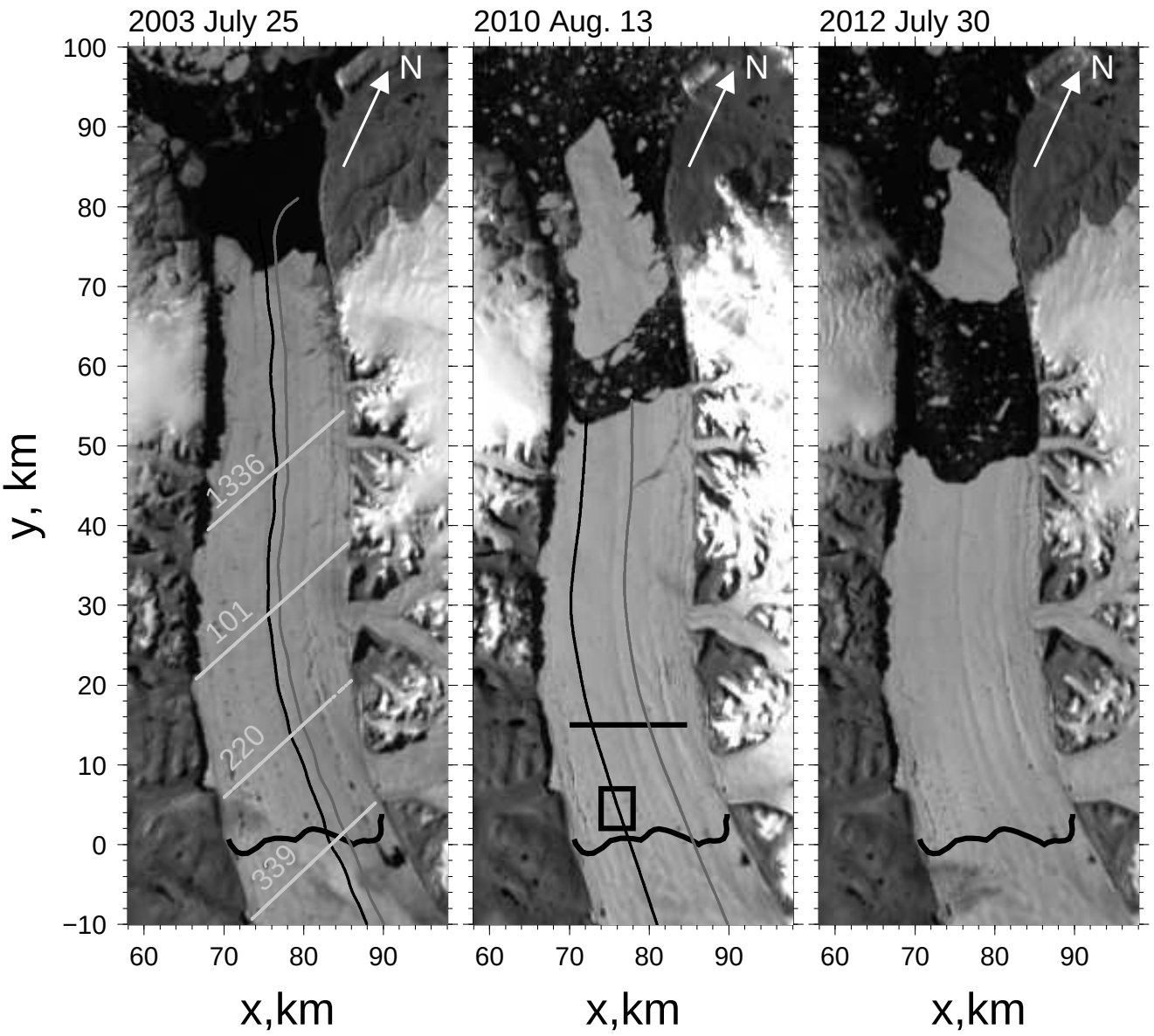


**Fig. 1.** Petermann Gletscher in 2003, 2010, and 2012 from MODIS Terra in rotated coordinate system. Repeat NASA flight tracks along fjord flown in 2002, 2003, 2007, and 2010 are shown in the left panel while 2011 flight tracks are shown in the middle panel. Light gray lines across the glacier are ICESat tracks. The thick black line across the glacier near y = 0 km is the grounding line location from *Rignot and Steffen* (2008). The horizontal black line near y = 15 km in the middle panel shows the location or MODIS surface reflectance profiles presented in Figure 6. The black rectangle shows an area of large and non-hydrostatic cravasses shown in Figure 10. Dark areas within 2 km off the western wall (x=70 km) are shadows cast by high terrain.

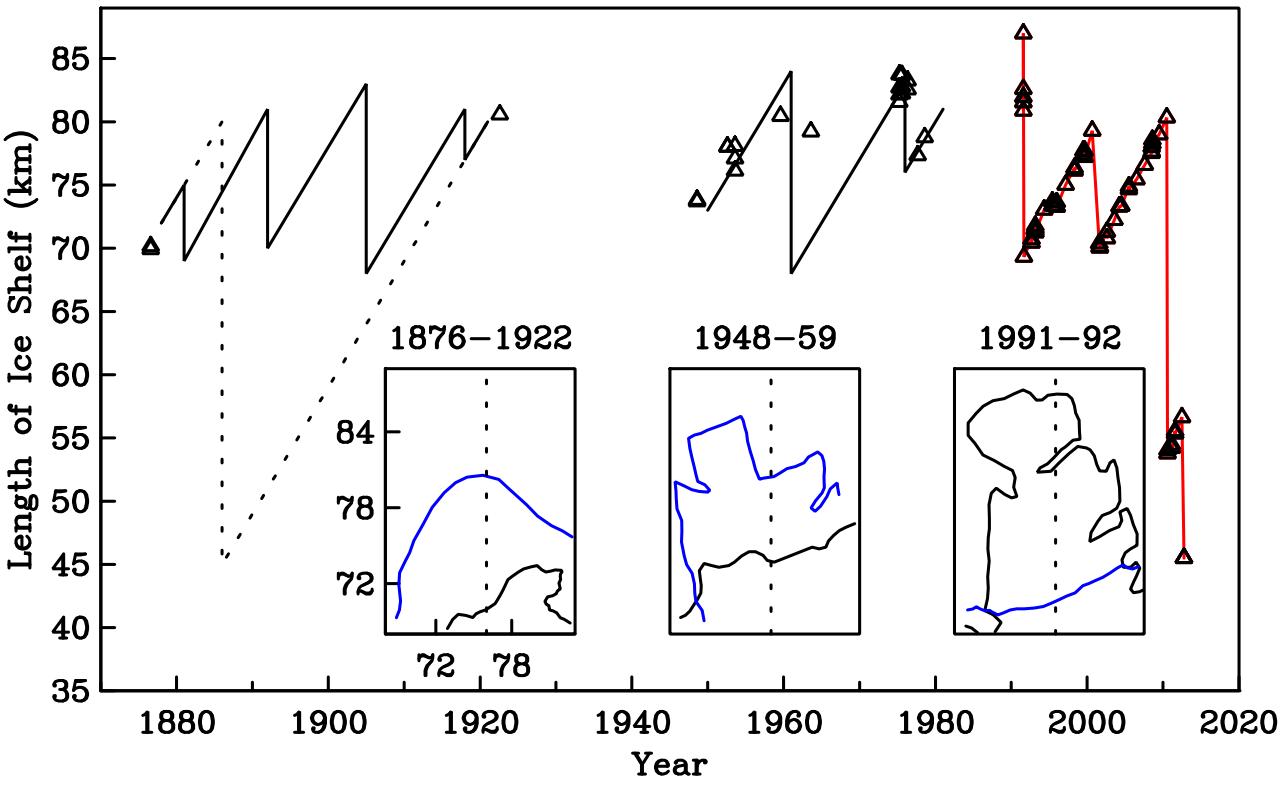


**Fig. 2.** Time series of the length of the ice shelf between near x=76 km. Selected profiles of terminus are shown as inserts (black first, blue second year). Co-ordinates (x,y) for inserts are same as Figure 1. Symbols indicate observations; dashed and solid time series show two alternate and hypothetical evolutions with the slope indicating a 1 km $a^{-1}$ advance of the terminus. Red line connects modern satellite data showing large calvings in 1991, 2001, 2010, and 2012.

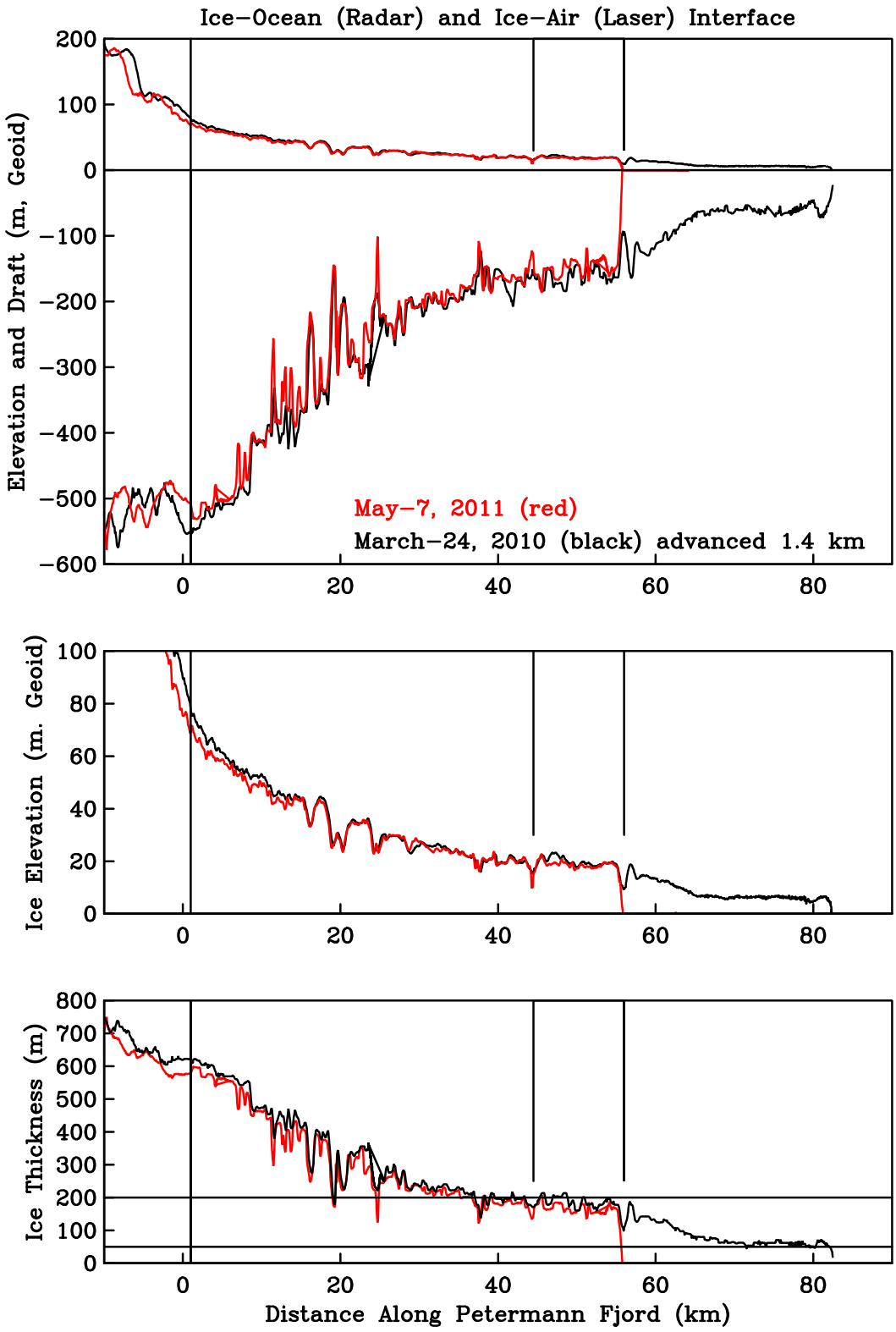


**Fig. 3.** Ice shelf profiles of Petermann Gletscher from CReSIS radar depth sounder and NASA's laser altimeter for May 7, 2011 and March 24, 2010 from repeat tracks along the ambient ice shelf (top). The ice surface elevation relative to EGM2008 geoid (middle) and ice thickness (bottom) reveal strong spatial correlation between years for a uniform 1.26 km $a^{-1}$ advance of the glacier. The glacier is grounded near y=1 km. The 2010 and 2012 break-up locations at y=56 km and y=44.5 km are indicated by vertical lines.

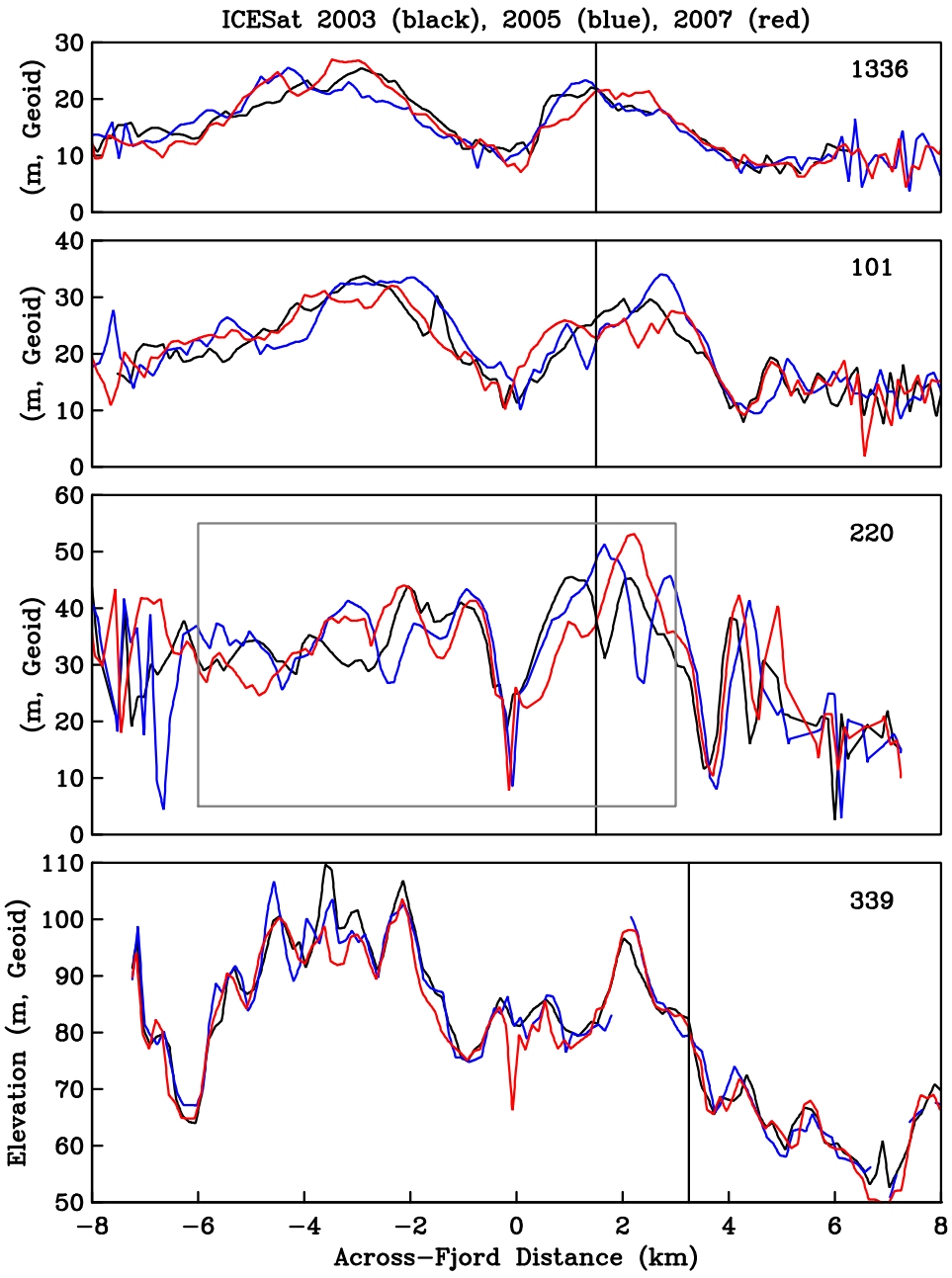


**Fig. 4.** Ice elevations from selected repeat ICESat tracks across Petermann Gletscher from north (track 1336, top) to south (track 339, bottom); see Figure 1 for locations. Across-fjord distance is shifted for each track (but not year) so that x'=0 indicates the time-mean location of the central channel. Vertical lines indicate cross-over location with airborne ATM track along the ambient ice shelf. Large grey boxed regions for track 220 indicates data used to generate Figure 5.

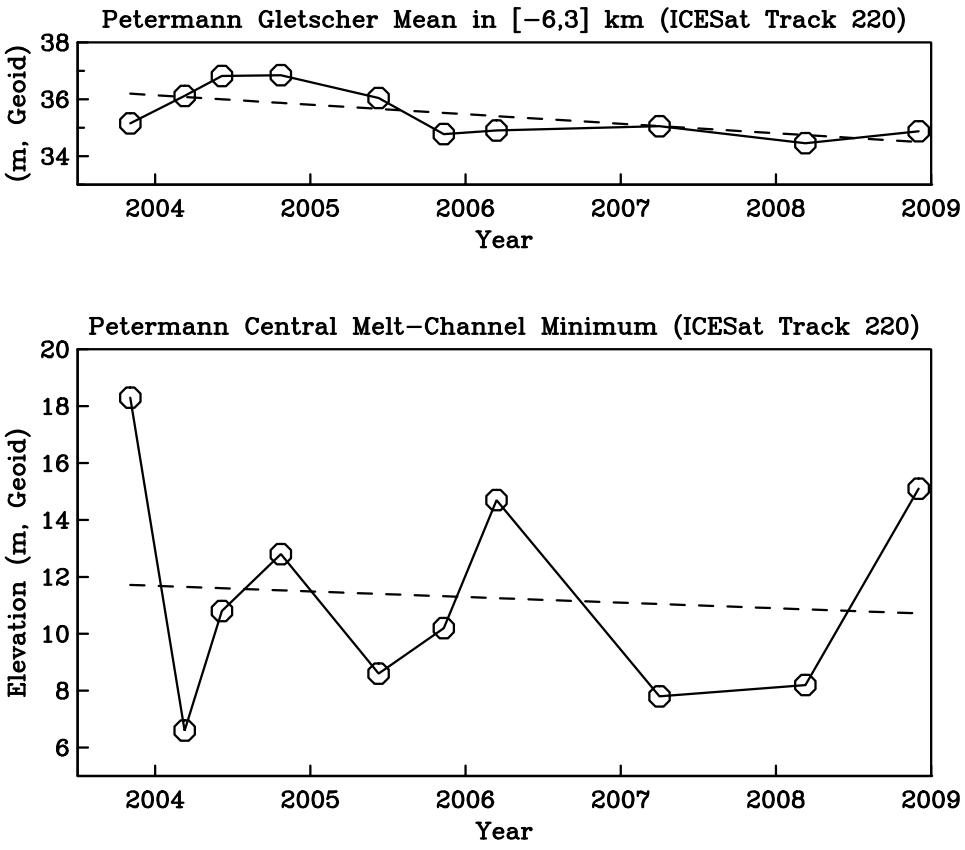


**Fig. 5.** Ice elevations from ICESat track 220 across Petermann Gletscher as the mean elevation along 9 km of track (top panel) and minimum elevation (bottom panel) over the central section of the glacier (see Figure 4 for the region of Track 220 that is used for these averages.) as a function of time. Dashed lines indicate the linear trend that is significantly different from zero at 95% confidence for the averaged (-0.33±0.26 m $a^{-1}$, top panel), but not the minimal elevation (-0.20±1.5 m $a^{-1}$, bottom panel).

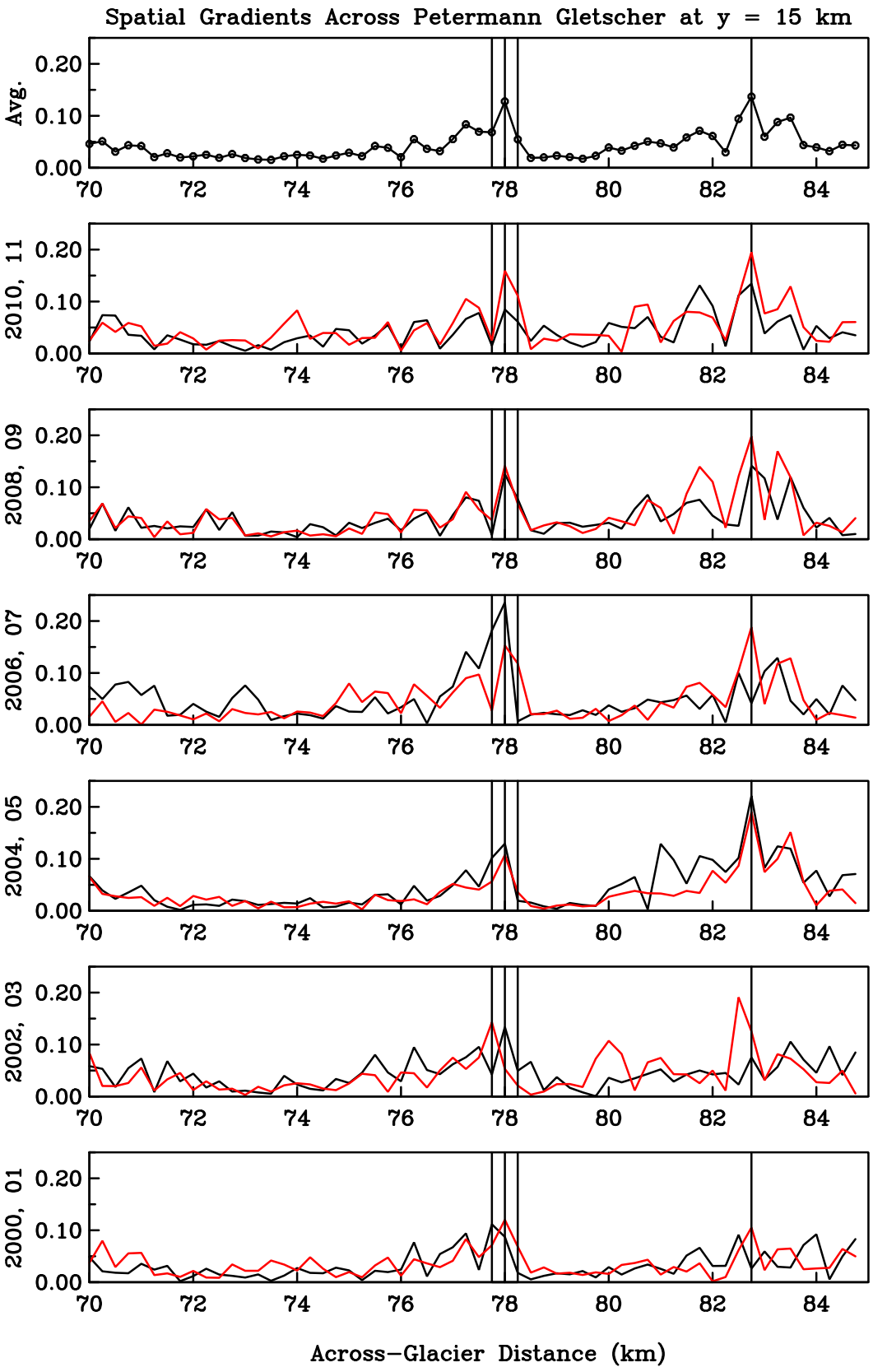


**Fig. 6.** Gradients of surface reflectance from MODIS-Terra across the glacier at y=15 km (see Figure 1 for location) from 2000 to 2011 with even (odd) years in black (red). Vertical lines indication location of the central channel ±1 pixel (∼250 m) near x=78 km and a large secondary channel near x=82.75 km.

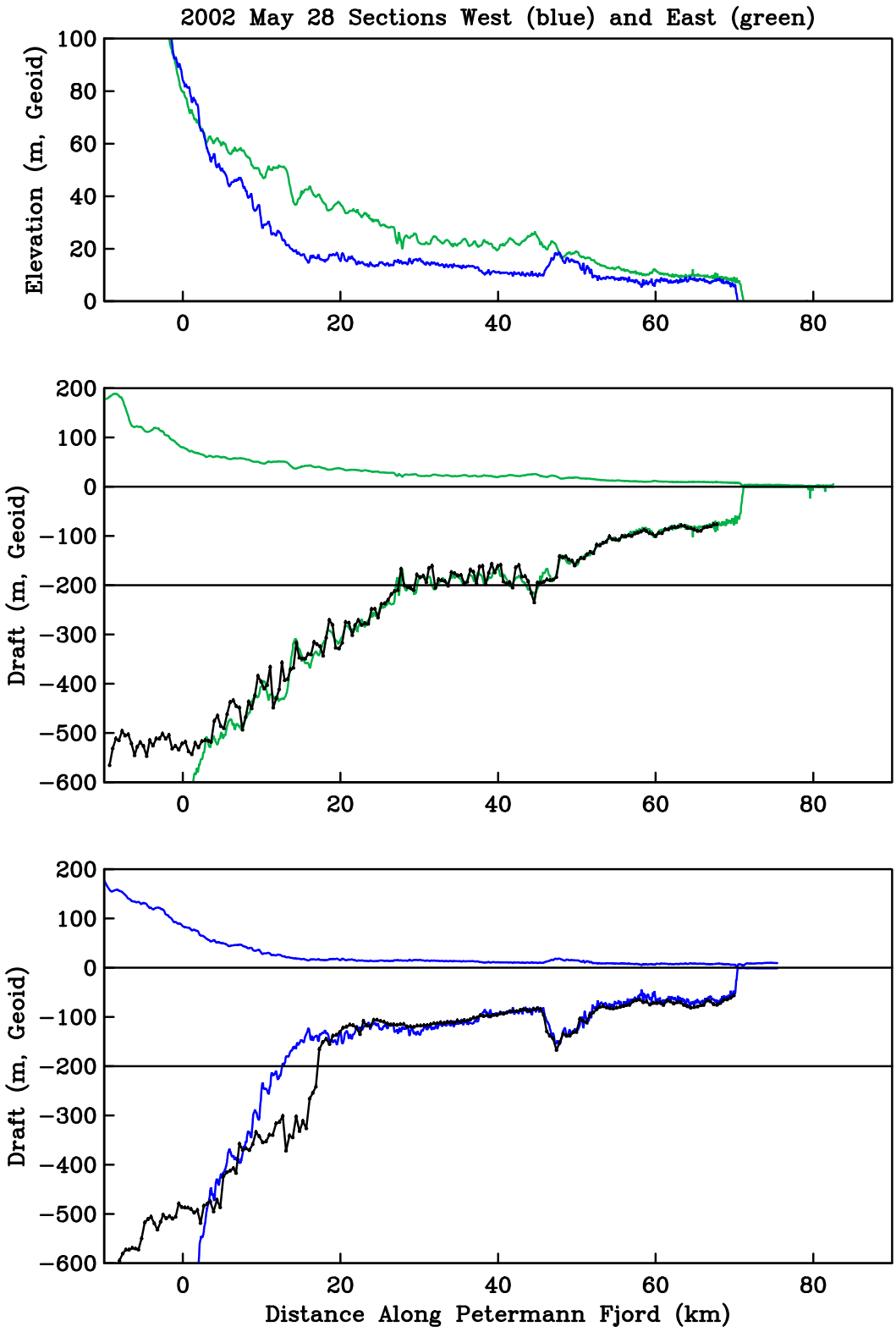


**Fig. 7.** Ice shelf profiles of Petermann Gletscher from CReSIS radar depth sounder for May 28, 2002 (black line) and Airborne Topographic Mapper (blue and green lines) relative to EGM2008 geoid. Colored bottom traces are ATM surface elevations scaled for hydrostatically floating ice.

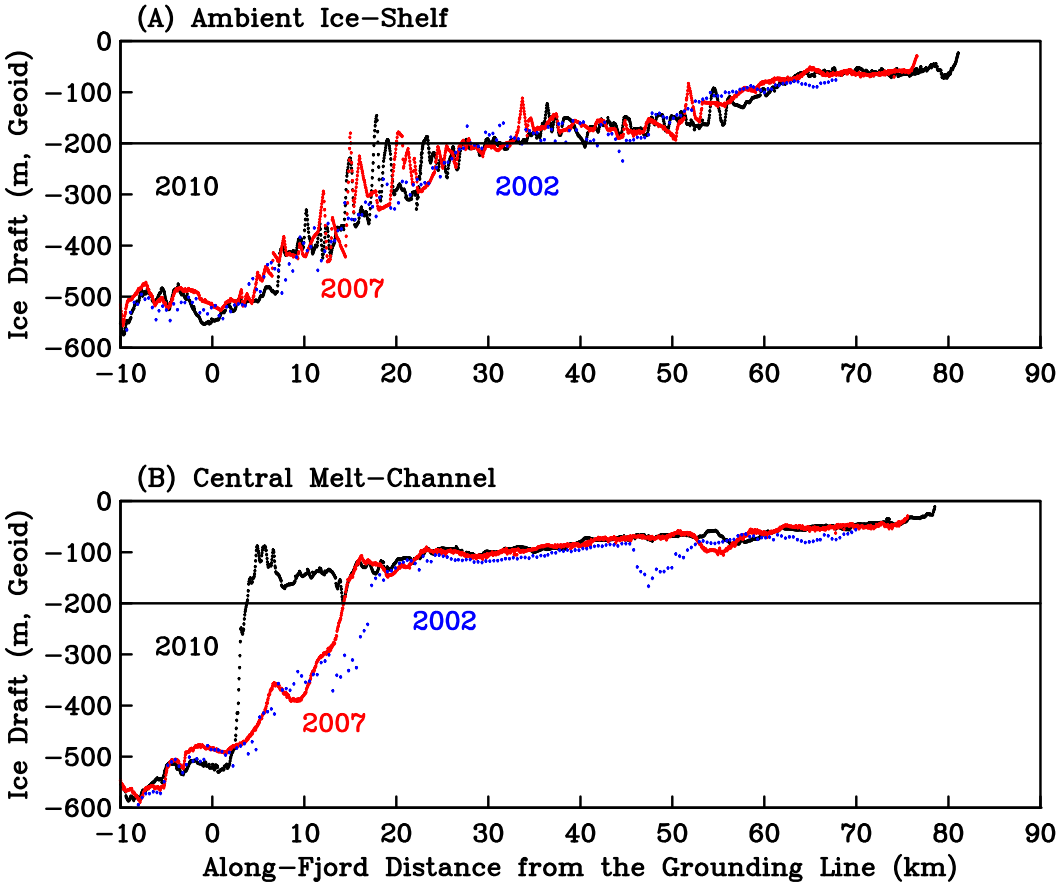


**Fig. 8.** Ice draft from CReSIS radar for (a) ambient ice shelf and (b) central melt-channel for 2002, 2007, and 2010. Notice the retreat and steepening of the central melt-channel towards the grounding line.

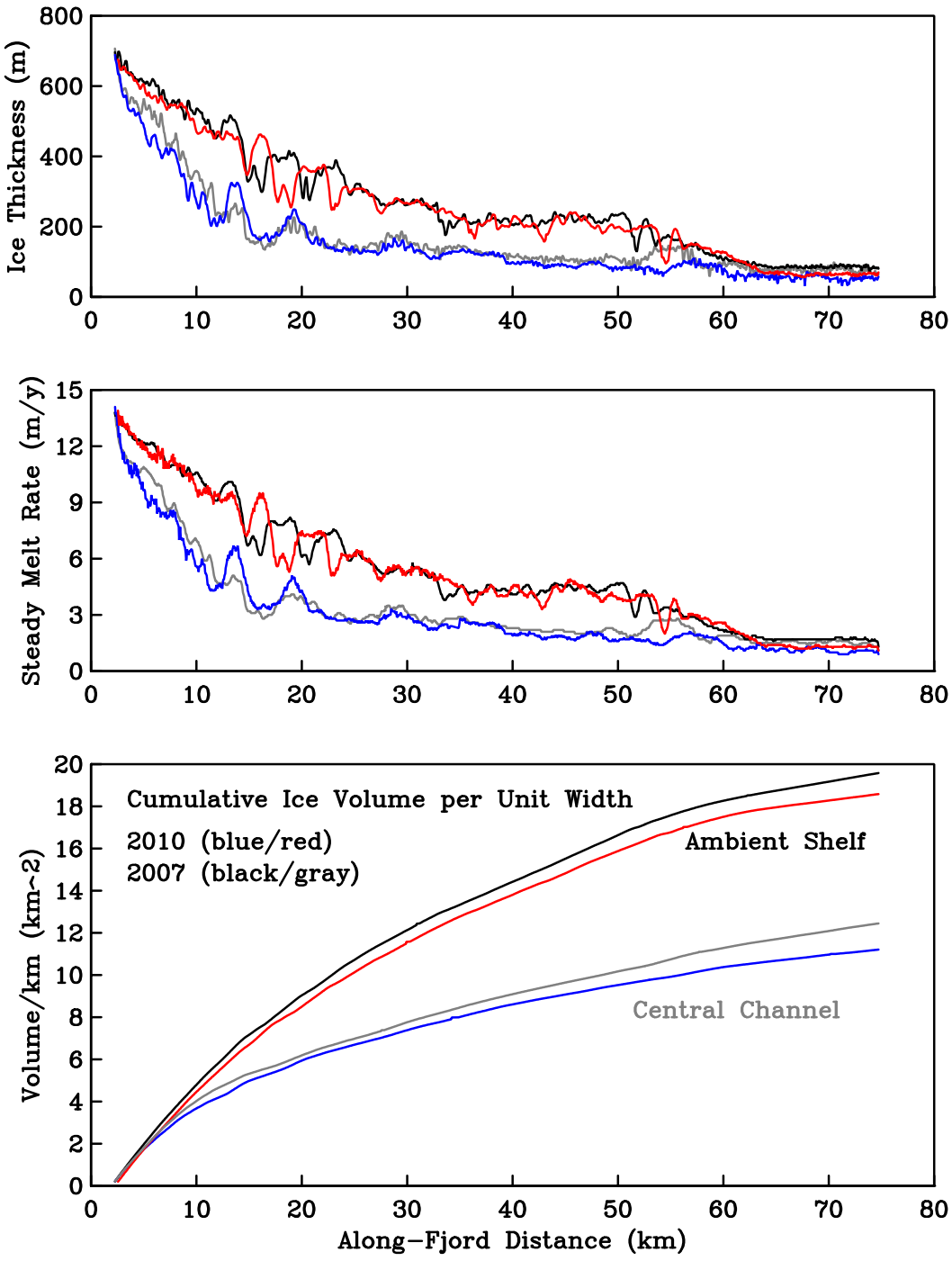


**Fig. 9.** Hydrostatic ice shelf profile of Petermann Gletscher from ATM in 2007 and 2010 (top), steady melt-rate (middle) and cumulative ice volume per unit width (bottom). The legend for each panel is provided in the bottom panel.

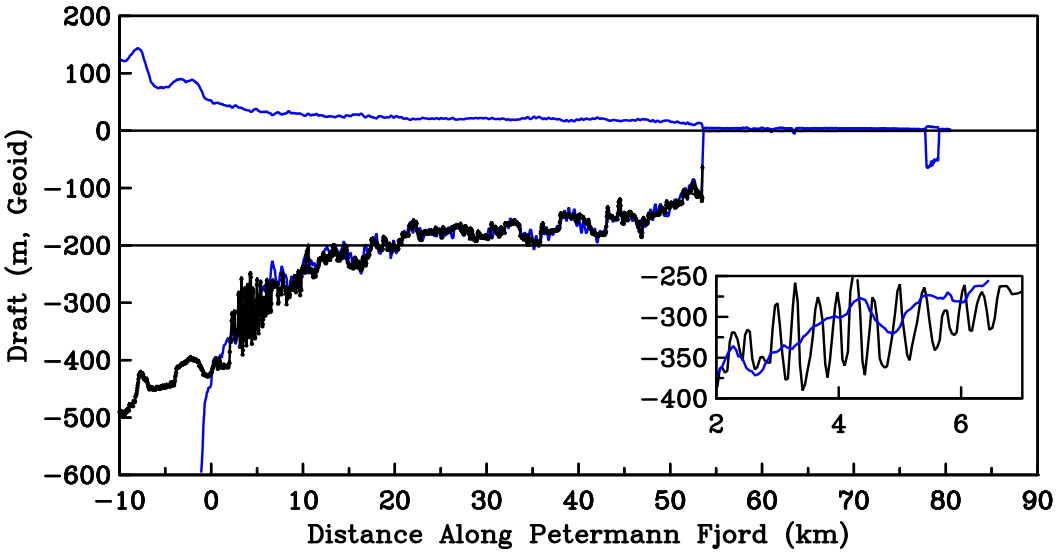


**Fig. 10.** Ice shelf profile of Petermann Gletscher from CReSIS radar depth sounder (black) and NASA's laser altimeter (blue) for May-7, 2011. The inset shows basal crevasses of 150 m vertical excursion embedded in 400 m thick floating ice near the grounding line. The blue line is surface elevation and draft of a hydrostatically floating ice shelf. Figure 1 shows the location of the insert.

**Table 1.** Petermann Gletscher radar data: Date, across-channel location ($x_i$), and regression parameters of radar ice thickness and radar surface elevations ($offset_i$ and $ratio_i$) along the central channel (i=1) and along the ambient ice shelf (i=2) for profiling radar and altimeter sections. Listed parameters are determined from data along a common 30 km long segment of floating ice shelf $y \in [21, 51]$ km; see Figure 1 for locations. Tidal elevation estimates are from *Padman and Erofeeva* (2004) for 81.25 N and 62 W.

| *Date* | $x_1(km)$ | $offset_1(m)$ | $ratio_1$ | $x_2(km)$ | $offset_2(m)$ | $ratio_2$ | $Tide(m)$ |
|---|---|---|---|---|---|---|---|
| 2011, May-7 | | | | 77.47 | -7.5 | 0.1065 | 0.08 |
| 2010, Mar.-24 | 76.02 | 2.9 | 0.1658 | 77.51 | 6.9 | 0.1325 | 0.15 |
| 2007, Sep.-13 | 76.08 | 532.4 | 0.1300 | 77.46 | 591.5 | 0.1154 | 0.15 |
| 2003, May-14 | 76.06 | 587.3 | 0.0800 | 77.48 | 574.8 | 0.0738 | 0.30 |
| 2002, May-28 | 76.06 | -29.7 | 0.1159 | 77.47 | -28.9 | 0.1007 | 0.13 |

**Table 2.** Petermann Gletscher radar and lidar data: Date and regression parameters of radar ice thickness and ATM elevations ($offset_i$ and $ratio_i$) along the central channel (i=1) and along the ambient ice shelf (i=2). Listed parameters are determined from data along a common 30 km long segment of floating ice shelf $y \in [21, 51]$ km; see Figure 1 and Table 1 for locations.

| *Date* | $offset_1(m)$ | $ratio_1$ | $offset_2(m)$ | $ratio_2$ |
|---|---|---|---|---|
| 2010, Mar.-24 | -4.0 | 0.131 | +0.5 | 0.103 |
| 2007, Sep.-13 | -0.9 | 0.123 | -0.0 | 0.115 |
| 2003, May-14 | -1.1 | 0.127 | +1.2 | 0.106 |

**Table 3.** Mean and standard deviation of ice thickness to the east and west of central channel for ICESat sections. See Figure 1 for locations and Figure 4 for selected across-glacier thickness profiles.

| Track | Years | Thickness East (m) | Thickness West (m) |
|---|---|---|---|
| 1336 | 6 | 16.5±5.0 | 12.7±4.6 |
| 101 | 7 | 23.0±5.5 | 17.5±6.2 |
| 220 | 10 | 33.4±6.0 | 30.9±11.7 |
| 339 | 9 | 87.2±10.7 | 71.8±11.7 |

**Table 4.** ATM-derived mass-balance estimates of net melt-rates (m $a^{-1}$) averaged along two repeat flow lines near the central channel and the ambient shelf from Eq.-5 for the ice shelf to the 2012 terminus, e.g., $y \in [2, 48]$ km. The flux-gate estimates are from *Rignot et al.* (2001) using radar interferometry and ATM data.

| | *Year* | $v_0 \sum_k \partial H_k/\partial y$ $(m\,a^{-1})$ | $\partial \widehat{H}/\partial t$ $(m\,a^{-1})$ | *Total* $(m\,a^{-1})$ | *Thickness* $(m)$ |
|---|---|---|---|---|---|
| *Central Channel* | 2007 | 4.9 | | | 217 |
| | 2010 | 4.8 | | | 203 |
| | $2007-2010$ | 4.9 | 5.0 | 9.9 | |
| *Ambient Shelf* | 2007 | 8.0 | | | 352 |
| | 2010 | 7.9 | | | 339 |
| | $2007-2010$ | 8.0 | 5.0 | 13.0 | |
| $ICESat-220$ | $2003-2009$ | | $3.1 \pm 2.4$ | | 330 |
| *Flux Gates* | 1999 | 8.4 | 0.8 | 9.2 | |